Check for updates

ChemPhotoChem

Chemistry Europe
European Chemical Societies Publishing
ChemPhotoChem

RESEARCH ARTICLE OPEN ACCESS Very Important Paper

Tunable Color Center Photoluminescence in Boron Nitride Nanotubes Through Reductive Arylation

Hiroki Nishinakama[1] | Hayato Saeki[1] | Naoki Tanaka[1,2,3] | Hayato Tateishi[1] | Koichiro Kato[1,2] | Koji Harano[1,4] | Koji Kimoto[4] | Tsuyohiko Fujigaya[1,2,3] | Tomohiro Shiraki[1,2,3]

[1]Department of Applied Chemistry, Graduate School of Engineering, Kyushu University, Fukuoka, Japan | [2]Center for Molecular Systems (CMS), Kyushu University, Fukuoka, Japan | [3]International Institute for Carbon-Neutral Energy Research (WPI-I2CNER), Kyushu University, Fukuoka, Japan | [4]Center for Basic Research on Materials, National Institute for Materials Science, Tsukuba, Ibaraki, Japan

Correspondence: Tsuyohiko Fujigaya (fujigaya.tsuyohiko.948@m.kyushu-u.ac.jp) | Tomohiro Shiraki (shiraki.tomohiro.992@m.kyushu-u.ac.jp)

Received: 18 May 2026 | **Revised:** 18 September 2026 | **Accepted:** 1 October 2026

Keywords: arylation | boron nitride nanotube | color center | defect | photoluminescence

ABSTRACT

Boron nitride nanotubes (BNNTs) are wide-bandgap one-dimensional nanomaterials that are promising hosts for defect-based luminescent material development. Herein, we report the formation and wavelength modulation of luminescent color centers (CCs) in BNNTs through reductive arylation. Phenyl-functionalized BNNTs exhibited new defect-related CC photoluminescence (PL) at 368 and 453 nm, respectively. Spectroscopic analyses revealed that arylation selectively formed B—C bonds, resulting in the introduction of sp^3 boron defects within the BN framework for luminescent CC formation. The emission properties were modulated by the defect density: increasing the degree of aryl functionalization enhanced the contribution of longer-wavelength emission, suggesting the formation of lower-energy defect states at proximal sp^3 boron defects. In addition, the CC PL wavelengths were further tuned by the electronic properties of *para*-substituents on the aryl groups, with electron-donating substituents inducing redshifted PL. Density functional theory calculations qualitatively supported that aryl functionalization reduces the calculated Kohn–Sham bandgap and that closely spaced sp^3 boron defects lead to a larger gap reduction than distant defects. These results demonstrate that reductive arylation provides a molecular defect-engineering strategy for controlling CC emission in BNNTs, offering a promising route toward chemically tunable nanoscale light sources based on functionalized boron nitride nanomaterials.

1 | Introduction

Boron nitride nanotubes (BNNTs) are one-dimensional (1D) nanocylinders composed of rolled-up hexagonal boron nitride (hBN) sheets [1–3]. In these materials, boron and nitrogen atoms are connected through sp^2-hybridized bonds, and the large electronegativity difference between B and N gives a partial ionic character in the covalent B—N bonds. As a result, BN materials, including BNNTs and hBN, exhibit wide bandgaps of approximately 5–6 eV. In contrast to carbon nanotubes (CNTs), whose electronic structures strongly depend on diameter and chirality, BNNTs maintain wide bandgap characteristics that are relatively insensitive to their structural differences because of the localized electronic structure of the B—N framework [1].

The wide bandgap and robust lattice structure of BN materials make them attractive host materials for nanoscale and quantum light sources. In pristine BN materials, excitonic luminescence is typically observed in the ultraviolet region; for example, Watanabe et al. reported that high-purity hBN single crystals exhibit luminescence at 215 nm, which is applicable to room-temperature deep-UV lasing [4]. In addition to such intrinsic band edge emission, localized lattice defects in hBN and BNNTs can act as color centers (CCs), introducing discrete defect states within the wide bandgap and enabling defect-derived CC photoluminescence

This is an open access article under the terms of the Creative Commons Attribution License, which permits use, distribution and reproduction in any medium, provided the original work is properly cited.

© 2026 The Author(s). *ChemPhotoChem* published by Wiley-VCH GmbH.

(PL) in the UV and visible regions [5, 6]. Thus, it is considered that defect structures could play a critical role in determining the optical properties of BNNTs. As an example of quantum emitters, single-photon emission from atomic defects in BNNTs has been experimentally demonstrated, showing bright and stable emission at room temperature [7]. Accordingly, the controlled formation and modulation of luminescent defects in BNNTs is an important strategy for developing chemically tunable light sources based on the wide-bandgap BN nanomaterials. Such BNNT CCs may be useful for UV–visible nanophotonic and anti-counterfeiting applications while also serving as chemically accessible model systems for understanding sp^3 defect physics in wide-bandgap BN nanomaterials.

Luminescent CCs consisting of atomic vacancies have been generated in BN materials by electron beam irradiation [8] and nitrogen-ion beam irradiation [9]. However, irradiation-based approaches often provide limited molecular-level control over the structure, density, and local chemical environment around the generated defects. We have recently reported a different strategy for producing CCs in BNNTs based on chemical functionalization [10]. In particular, reductive alkylation of BNNTs selectively attaches hexyl groups to boron atoms in the BN framework, resulting in the formation of sp^3 boron defects. The defect generates luminescent CCs that exhibit lower-energy UV and visible PL compared with the intrinsic band edge emission of BNNTs. Recent theoretical calculations have also suggested that sp^3-hybridized defect pairs in BN materials, including BNNTs and hBN, can generate optically active defect transitions with substantially lower energies than the intrinsic bandgap transition [11]. These findings indicate that molecularly designed defect formation is promising for bandgap engineering and wavelength modulation in BN nanomaterials.

In this study, reductive arylation, a reaction widely used for the chemical functionalization of CNTs [12, 13], was applied to generate luminescent CCs in BNNTs (Figure 1). Arylated BNNTs exhibited PL in the UV and visible regions at 368 and 453 nm, respectively. In addition, this functionalization strategy allowed us to identify key structural parameters for modulating the PL wavelength of the generated CCs: namely, the density and spatial proximity of the introduced defects and the electronic properties of substituents on the functionalized aryl groups. Theoretical simulations qualitatively supported the experimental interpretation, showing that aryl functionalization modifies the ground-state electronic structure of BNNTs and that proximal defect formation leads to a larger reduction in the calculated Kohn–Sham gap. These results demonstrate that reductive arylation provides a molecular defect-engineering strategy for tuning the optical properties of BNNTs.

2 | Results and Discussion

2.1 | Synthesis of Arylated BNNTs and Their Optical Properties

For arylation, BNNTs were dispersed in dehydrated tetrahydrofuran (THF) containing sodium and naphthalene to generate sodium naphthalenide, followed by the addition of bromobenzene. After stirring for 48 h, the reaction was quenched by adding methanol and water to the mixture. The resulting precipitate was collected and washed by filtration to obtain phenyl-functionalized BNNTs (ph-BNNTs) (for details, see Section 4).

For optical characterization, BNNTs and ph-BNNTs were dispersed in aqueous solutions of 0.01 wt% cetyltrimethylammonium bromide (CTAB). Figure 2 shows the PL spectra of BNNTs and ph-BNNTs. For BNNTs, a PL peak was observed at 330 nm, which is assignable to atomic vacancies or impurities (carbon or oxygen) [5, 6]. In contrast, ph-BNNTs exhibited PL peaks at 368 and 453 nm. These emissions were not observed in control experiments performed under otherwise identical reaction conditions: (i) without bromobenzene, where only reduction of BNNTs by sodium naphthalenide occurred and (ii) using toluene, which has no bromo group, instead of bromobenzene (Figure S1). These results indicate that reductive treatment itself, possible side reactions during reduction, or noncovalent interaction with aromatic molecules are unlikely to be the main origins of the newly observed luminescent CCs in ph-BNNTs. Namely, the results indicate that luminescent CCs were formed by the arylation of BNNTs with bromobenzene. In addition, these emission wavelengths for ph-BNNTs were redshifted compared with those of CC PL from alkylated BNNTs

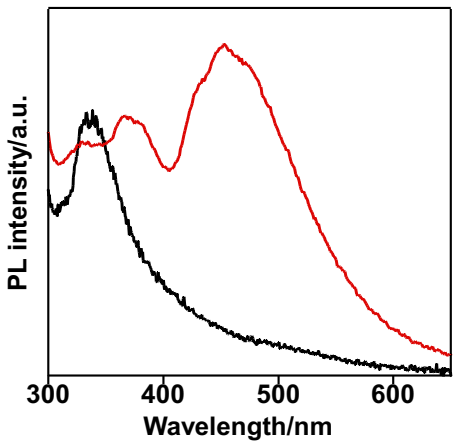


FIGURE 2 | PL spectra of BNNTs (black) and ph-BNNTs (red) dispersed in aqueous CTAB solutions. $\lambda_{ex} = 200$ nm.

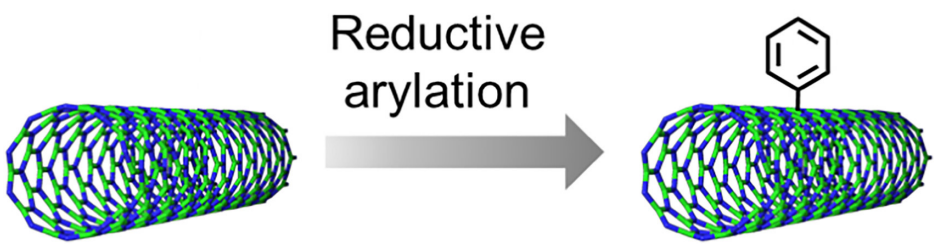


FIGURE 1 | Schematic illustration of the arylation of BNNTs.

23670932, 2026, 10, Downloaded from https://chemistry-europe.onlinelibrary.wiley.com/doi/10.1002/cptc.70316 by National Institute For, Wiley Online Library on [15/10/2026]. See the Terms and Conditions (https://onlinelibrary.wiley.com/terms-and-conditions) on Wiley Online Library for rules of use; OA articles are governed by the applicable Creative Commons License

(334 and 413 nm) [10], suggesting that the CC energy levels could be modulated depending on the attached organic groups.

In the UV–vis absorption spectrum of BNNTs (Figure 3a), a sharp peak was observed at 204 nm, which is attributed to the bandgap transition. For ph-BNNTs, the absorbance increased in the 210–350 nm region. The generation of additional absorption bands was observed at 219, 273, and 350 nm clearly in the subtraction spectrum between ph-BNNTs and BNNTs (Figure 3b). This result indicates that defect introduction through arylation partially modifies the electronic structures of the functionalized regions of BNNTs, leading to CC formation. Furthermore, excitation spectra of ph-BNNTs for the emissions at 368 and 453 nm (Figure S2) showed that these emissions were generated not only by excitation of the bandgap transition at 205 nm but also by excitation of the lower-energy absorption bands around 275 and 350 nm observed in absorption spectroscopy. The contribution of the bandgap transition to these longer wavelength emissions indicates exciton trapping at the CCs to generate CC PL in ph-BNNTs, as also suggested for hexylated BNNTs [10].

To investigate the defect structures introduced by arylation for CC formation in ph-BNNTs, X-ray photoelectron spectroscopy (XPS), Fourier transform infrared spectroscopy (FT-IR), and thermogravimetric analysis (TG) were performed. Figure 4 shows the XPS spectra of the B 1s and N 1s orbitals for BNNTs and ph-BNNTs, analyzed by peak deconvolution using Gaussian–Lorentzian mixed functions. Both BNNTs and ph-BNNTs exhibited clear peaks at 189 and 397 eV in the B 1s and N 1s spectra, respectively, corresponding to B—N bond in the BN network [14]. A signal at 190 eV, attributable to B—O bonds, was observed for both BNNTs and ph-BNNTs and is likely associated with oxidized species, such as residual B_2O_3 generated during the purification process [15]. Notably, ph-BNNTs showed an additional peak at 187 eV in the B 1s region, which was assigned to B—C bond. In contrast, no signal related to N—C bond was detected. These results indicate the selective formation of sp^3 boron defects by arylation. This selectivity would be derived from the reaction process in which electrons transferred from sodium naphthalenide to BNNTs localize in the empty p orbitals of B atoms and subsequently react with aryl radicals to form B—C bond, similar to the behavior observed in reductive alkylation [10].

The FT-IR spectra of BNNTs and ph-BNNTs (Figure S3) showed peaks at 786 and 1359 cm^{-1}, which were assigned to the out-of-plane B—N—B bending mode and the in-plane B—N stretching mode of the BN framework, respectively [14–16]. In addition, ph-BNNTs exhibited peaks around 1100 and 3300 cm^{-1}, which were not observed for BNNTs. These signals were attributed to vibrational modes associated with B—C bond formation and C—H stretching modes of aromatic rings, respectively [10, 14], further supporting the arylation of BNNTs through this reaction.

The degree of functionalization was evaluated by TG analysis (Figure S4). BNNTs exhibited thermal stability above 800 °C. In contrast, ph-BNNTs showed a weight loss of 6.9 wt% at around 200–400 °C, arising from the degradation and removal of the functionalized aryl groups. Based on this weight loss, the degree of functionalization was estimated to be approximately one aryl group per 43 B—N bonds in ph-BNNTs. The retention of the tubular structure after the arylation reaction was confirmed by transmission electron microscopy observations of ph-BNNTs (Figure S5).

When hBN powder was used instead of BNNTs for the arylation reaction, redshifted PL was not generated (Figure S6a). In addition, FT-IR, TG, and XPS analyses of hBN treated with sodium naphthalenide and bromobenzene showed no detectable signals attributable to arylation, such as B—C bond formation, aromatic C—H stretching, or decomposition of covalently attached organic groups (Figure S6b–d). This result indicates that the curvature of the BNNT walls enhances their reactivity, thereby facilitating CC formation under these reaction conditions.

Accordingly, these results demonstrate that reductive arylation of BNNTs introduces sp^3 boron defects, resulting in the formation of CCs that exhibit redshifted emissions.

2.2 | Dependence of CC Emission Properties on Defect Density in ph-BNNTs

As defect introduction by arylation is key to CC formation, we investigated the dependence of CC PL properties on the defect density. Thus, ph-BNNTs were synthesized under similar arylation conditions, except that the amount of bromobenzene used in the reaction was changed to 0.5-fold or

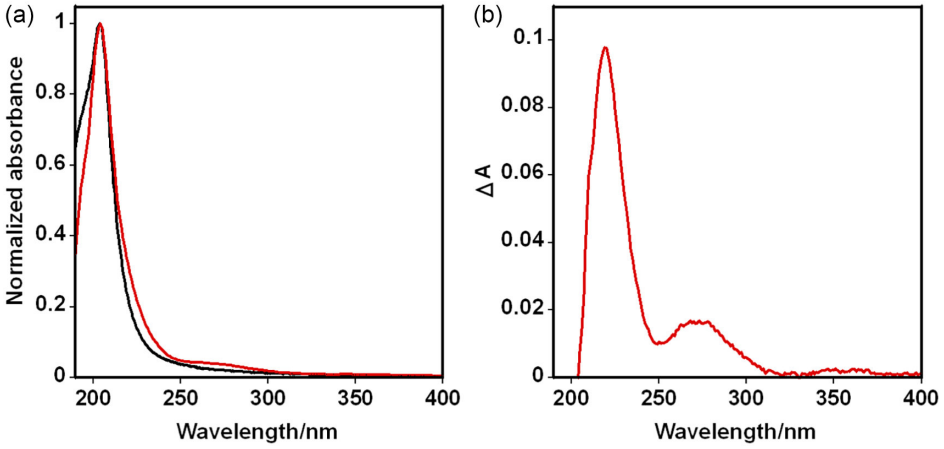


FIGURE 3 | (a) Absorption spectra of BNNTs (black) and ph-BNNTs (red) dispersed in aqueous CTAB solutions and (b) the difference absorption spectrum obtained by subtracting the BNNT spectrum from the ph-BNNT spectrum.

23670932, 2026, 10, Downloaded from https://chemistry-europe.onlinelibrary.wiley.com/doi/10.1002/cptc.70316 by National Institute For, Wiley Online Library on [15/10/2026]. See the Terms and Conditions (https://onlinelibrary.wiley.com/terms-and-conditions) on Wiley Online Library for rules of use; OA articles are governed by the applicable Creative Commons License

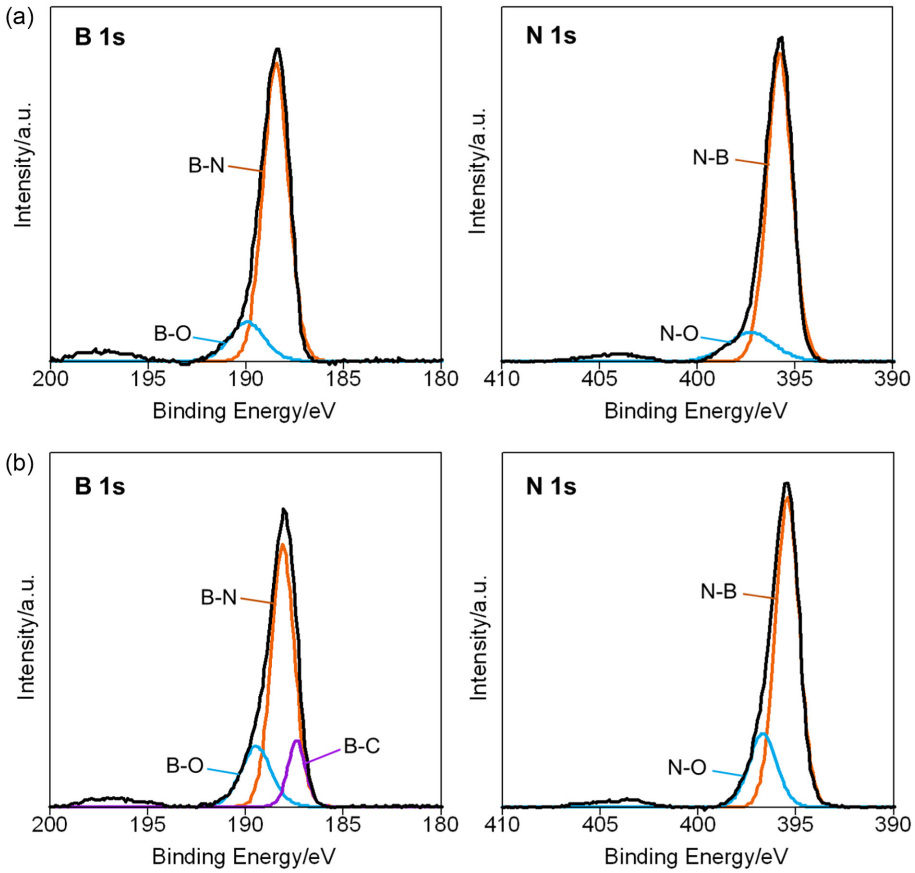


FIGURE 4 | XPS spectra of the B 1s and N 1s of (a) BNNTs and (b) ph-BNNTs.

5-fold relative to the standard condition (ph-BNNTs_0.5 and ph-BNNTs_5, respectively).

Figure 5a shows the PL spectra of ph-BNNTs_0.5 and ph-BNNTs_5. As described in the previous section, ph-BNNTs exhibited two PL peaks at 368 and 453 nm. For ph-BNNTs_0.5, the main peak appeared at 377 nm. In contrast, ph-BNNTs_5 showed a main peak at 457 nm, while the PL intensity at around 377 nm decreased. TG analysis indicates that the weight loss percentages corresponding to the amount of functionalized aryl groups were 2.0%, 6.9%, and 14.6% for ph-BNNTs_0.5, ph-BNNTs, and ph-BNNTs_5, respectively. To assess the batch-to-batch variation in the arylation reaction, TG measurements were performed for two independently synthesized samples

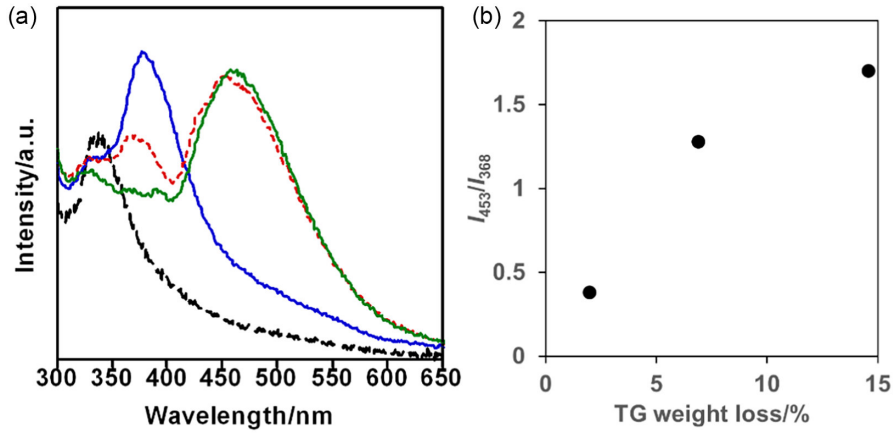


FIGURE 5 | (a) PL spectra of ph-BNNTs_0.5 (blue) and ph-BNNTs_5 (green) dispersed in aqueous CTAB solutions. The spectra of BNNTs (black) and ph-BNNTs (red), which are the same as those shown in Figure 2, are also shown for comparison. $\lambda_{ex} = 200$ nm. The TG weight loss values of the representative samples used for the PL measurements were 2.0, 6.9, and 14.6 wt% for ph-BNNTs_0.5, ph-BNNTs, and ph-BNNTs_5, respectively. (b) PL intensity ratio of the emissions at 453 and 368 nm (I_{453}/I_{368}) as a function of the weight loss percentage associated with the amount of functionalized aryl groups in ph-BNNTs_0.5, ph-BNNTs, and ph-BNNTs_5. Absorbance-normalized PL spectra of ph-BNNTs_0.5, ph-BNNTs, and ph-BNNTs_5, obtained using the absorbance at 200 nm, are shown in Figure S7.

23670932, 2026, 10, Downloaded from https://chemistry-europe.onlinelibrary.wiley.com/doi/10.1002/cptc.70316 by National Institute For, Wiley Online Library on [15/10/2026]. See the Terms and Conditions (https://onlinelibrary.wiley.com/terms-and-conditions) on Wiley Online Library for rules of use; OA articles are governed by the applicable Creative Commons License

for each functionalization condition. The average TG weight losses attributed to functionalized aryl groups were estimated to be 3.1 ± 1.6, 5.4 ± 2.1, and 12.5 ± 2.9 wt% for ph-BNNTs_0.5, ph-BNNTs, and ph-BNNTs_5, respectively (Table S1). Although noticeable batch-to-batch variation was observed, particularly for the lower and standard bromobenzene conditions, the high-bromobenzene condition gave a larger average TG weight loss. In addition, XPS-derived atomic concentration analysis showed that the C/B ratio increased with increasing amount of bromobenzene used in the reaction, while the N/B ratio remained almost unchanged (Table S2), further supporting the increase in the aryl groups covalently attached to the ph-BNNT series. Then, the ratio of the PL intensity at 453 nm to that at 368 nm was plotted as a function of the TG weight loss percentage corresponding to the aryl group content (Figure 5b). The plot suggests a qualitative defect density-dependent trend in which the relative contribution of the longer wavelength emission increases under higher aryl functionalization conditions. This trend was also confirmed in the absorbance-normalized PL spectra, in which the PL intensities were normalized using the absorbance at 200 nm (Figure S7). This result indicates that, at a lower degree of functionalization, the aryl groups are sparsely distributed on the BNNT walls, generating CCs that emit around 370 nm. In contrast, at a higher degree of functionalization, the probability of forming proximal aryl-functionalized sites increases. Such proximal defect sites may strongly affect the electronic structures of the CCs, leading to redshifted PL at around 455 nm. To examine this hypothesis, a divalent modifier, 1,8-bis(bromomethyl)naphthalene, was used as a reactant for BNNT functionalization. The resulting functionalized BNNTs exhibited a main PL peak at 449 nm, while no obvious peak was detected around 368 nm (Figure S8) (Note: the PL around 330 nm is assigned to emission derived from vacancy defects originally present in the BNNTs, as mentioned above). This experiment does not directly prove the formation of neighboring boron-functionalized sites. However, it supports the possibility that the introduction of closely spaced defects contributes to the generation of longer-wavelength CC PL. Furthermore, theoretical simulations, described in detail in the following section, also support the generation of redshifted CC PL by proximal aryl functionalization in ph-BNNTs. Although the number of functionalization levels examined in this study is limited, these results suggest a defect density-dependent trend in which the relative contribution of the longer-wavelength CC PL increases with increasing aryl functionalization degree.

Accordingly, these results suggest that defect density can be one of the factors influencing the electronic structures and PL wavelengths of CCs formed in functionalized BNNTs.

2.3 | PL Wavelength Modulation Through Substituent Effects of the Functionalized Aryl Groups

We next investigated the effects of substituents on the aryl groups on the CC PL properties of arylated BNNTs. As arylation reagents, *p*-bromotoluene and 4-bromo-*N*,*N*-dimethylaniline were used instead of bromobenzene to synthesize BNNTs functionalized with tolyl and 4-(*N*,*N*-dimethylamino)phenyl groups, respectively (denoted as tol-BNNTs and dma-BNNTs).

Figure 6a shows the PL spectra of tol-BNNTs and dma-BNNTs. These samples had defect amounts comparable to those of ph-BNNTs, as indicated by their similar TG weight loss percentages of 8.8% and 6.6% for tol-BNNTs and dma-BNNTs, respectively. tol-BNNTs showed PL peaks at 386 and 465 nm, whereas dma-BNNTs showed peaks at 424 and 539 nm. Both emissions appearing in the shorter- and longer-wavelength regions were redshifted compared with those of ph-BNNTs (368 and 453 nm, respectively). In Figure 6b, the emission energies of the observed CC PL were plotted as a function of the Hammett substituent constants of the *para*-substituents on the functionalized aryl groups, in which substituent-dependent trends were observed for both emission regions. Substituent-dependent PL spectral shifts have been reported for CCs formed in single-walled CNTs [17], where the character of sp^3 carbon defects was modulated depending on the electronic properties of *para*-substituents, resulting in tunable emission wavelengths [18]. In arylated BNNTs, such modulation of the sp^3 boron defect character based on the electronic properties of the aryl substituents may occur, leading to changes in the CC electronic

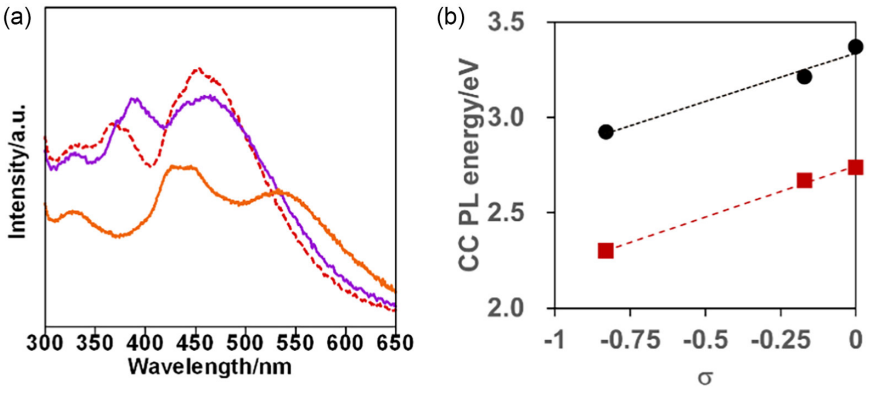


FIGURE 6 | (a) PL spectra of tol-BNNTs (purple) and dma-BNNTs (orange) dispersed in aqueous CTAB solutions. The spectrum of ph-BNNTs (red), which is the same as that shown in Figure 2, is also shown for comparison. $\lambda_{ex} = 200$ nm. (b) Relationship between PL emission energies and Hammett substituent constants for the shorter-wavelength emission peaks (black circles) and longer-wavelength emission peaks (red squares). The dashed lines represent linear regression fits, with R^2 values of 0.975 and 0.998 for the shorter- and longer-wavelength emissions, respectively; these fits are provided as visual guides for the observed trends.

23670932, 2026, 10, Downloaded from https://chemistry-europe.onlinelibrary.wiley.com/doi/10.1002/cptc.70316 by National Institute For, Wiley Online Library on [15/10/2026]. See the Terms and Conditions (https://onlinelibrary.wiley.com/terms-and-conditions) on Wiley Online Library for rules of use; OA articles are governed by the applicable Creative Commons License

structures and PL wavelengths. The present result, obtained from three different aryl substituents, should be regarded as a preliminary substituent-dependent trend rather than a general Hammett relationship. Although the samples were prepared under comparable reaction conditions, subtle differences in functionalization degree and defect distribution may also contribute to the observed emission energy shifts. Further studies using additional electron-donating and electron-withdrawing substituents compatible with the present reductive arylation conditions, together with replicate measurements and statistical analyses, will be required to clarify the correlation between substituent electronic properties and the emission energies of BNNT CCs.

2.4 | Electronic Structure Evaluation of Arylated BNNTs Based on Theoretical Simulations

Density functional theory (DFT) calculations were performed using the Vienna ab initio simulation package (VASP) to investigate the electronic structure changes in BNNTs induced by arylation. The generalized gradient approximation (GGA) with the Perdew–Burke–Ernzerhof (PBE) exchange–correlation functional was employed. A single-walled zigzag (10,0) BNNT was used as the model structure. The calculation cell contained one BNNT unit consisting of 240 atoms, including 120 boron atoms and 120 nitrogen atoms.

Figure 7a shows the calculated band structures of the structurally optimized BNNT and ph-BNNT. The calculated Kohn–Sham bandgaps of BNNT and ph-BNNT were 4.01 and 3.57 eV, respectively. In both models, the valence band maximum (VBM) and conduction band minimum (CBM) were located at the Γ point. Visualization of the wave functions of ph-BNNT (Figure 7b) revealed that the wave functions were localized around the sp^3 boron defect in the BNNT wall rather than on the functionalized phenyl group. These results indicate that the introduction of sp^3 boron defects through phenyl functionalization modifies the ground-state electronic structure of BNNTs and reduces the

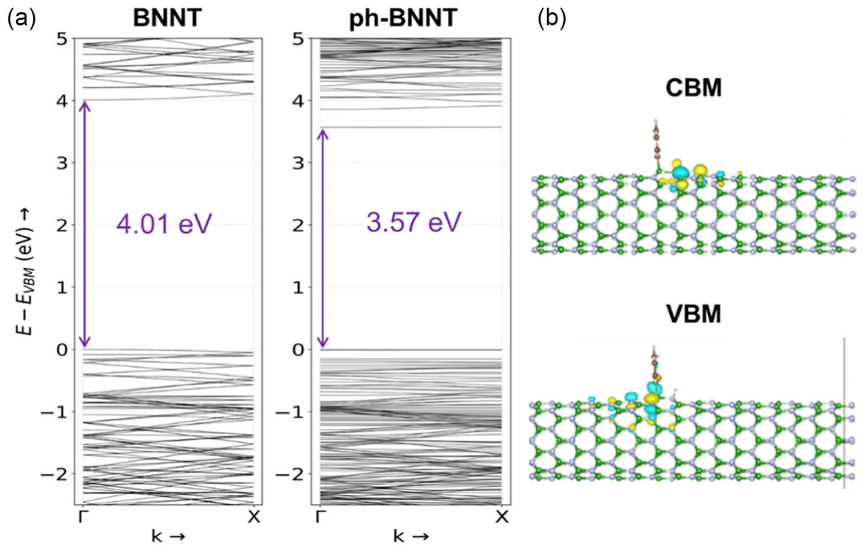


FIGURE 7 | (a) Calculated band structures of BNNT and ph-BNNT and (b) wave functions corresponding to the VBM and CBM of ph-BNNT.

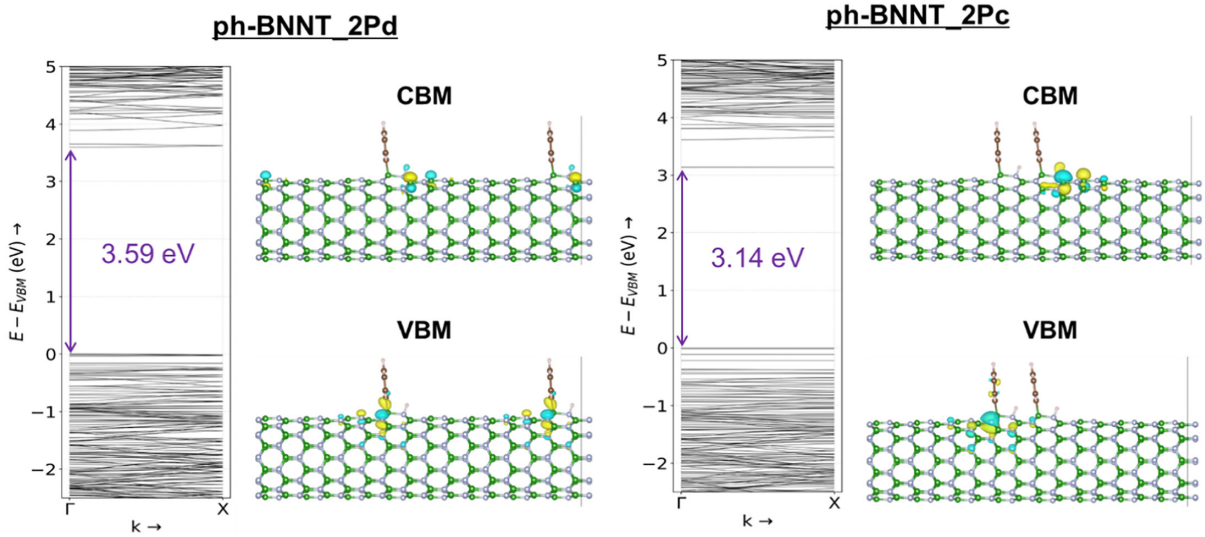


FIGURE 8 | Calculated band structures and wave functions corresponding to the VBM and CBM of ph-BNNT_2Pd and ph-BNNT_2Pc.

23670932, 2026, 10, Downloaded from https://chemistry-europe.onlinelibrary.wiley.com/doi/10.1002/cptc.70316 by National Institute For, Wiley Online Library on [15/10/2026]. See the Terms and Conditions (https://onlinelibrary.wiley.com/terms-and-conditions) on Wiley Online Library for rules of use; OA articles are governed by the applicable Creative Commons License

calculated Kohn–Sham bandgap. Given the limitation of PBE for absolute bandgap values, the magnitude of this reduction should be interpreted qualitatively; nevertheless, the trend is consistent with the experimentally observed redshifted PL.

Next, the effect of proximal sp^3 boron defect formation on the electronic structures of functionalized BNNTs was examined using bifunctionalized models bearing two phenyl groups on the BNNT wall at distant or close positions, denoted as ph-BNNT_2Pd and ph-BNNT_2Pc, respectively. Figure 8 shows the calculated band structures and wave functions corresponding to the VBM and CBM of ph-BNNT_2Pd and ph-BNNT_2Pc, respectively. At the Γ point, the bandgap of ph-BNNT_2Pd was estimated to be 3.59 eV, which is comparable to that of ph-BNNT (3.57 eV). In contrast, ph-BNNT_2Pc exhibited a smaller Kohn–Sham bandgap of 3.14 eV. Furthermore, in ph-BNNT_2Pd, the wave functions of the VBM and CBM were localized separately around each sp^3 boron defect. By contrast, in ph-BNNT_2Pc, the VBM and CBM wave functions were localized around one of the closely spaced sp^3 boron defect sites. These results suggest that proximal sp^3 boron defects more strongly perturb the ground-state electronic structure and reduce the calculated Kohn–Sham gap relative to distant defects. This qualitative trend is consistent with the experimentally observed defect-amount-dependent redshift in PL.

Regarding the substituent effect, the present ground-state PBE calculations gave almost identical Kohn–Sham bandgaps for ph-BNNT, tol-BNNT, and dma-BNNT, namely, 3.57, 3.59, and 3.58 eV, respectively. Thus, the experimentally observed substituent-dependent PL shifts are not reproduced within the present computational framework. Because the observed emission involves excited-state processes and may be influenced by excitonic and/or charge-transfer effects, the microscopic origin of the substituent dependence cannot be determined from the present ground-state calculations and remains an open question for future theoretical study.

3 | Conclusion

In conclusion, reductive arylation of BNNTs successfully generated luminescent CCs, giving rise to defect-related CC PL at 368 and 453 nm in ph-BNNTs. XPS and FT-IR analyses revealed that aryl functionalization selectively formed B—C bonds, resulting in the introduction of sp^3 boron defects within the B—N framework. The electronic structure modification of BNNTs by the defect introduction was confirmed in UV–vis absorption spectroscopy, and PL excitation measurements suggested a CC PL emission process through exciton trapping at the CCs in ph-BNNTs.

The generated CC PL wavelengths showed a defect density-dependent trend: increasing the degree of aryl functionalization enhanced the contribution of the longer wavelength emission around 453–457 nm, suggesting that proximal sp^3 boron defects may contribute to the formation of lower-energy CC states. This interpretation was qualitatively supported by the DFT calculations, which showed a smaller Kohn–Sham gap for the proximal defect model than for the distant defect model. The present DFT results should therefore be regarded as a qualitative description of ground-state electronic structure changes associated with defect introduction and proximity rather than as quantitative predictions of PL transition energies.

The PL wavelengths were also modulated by the electronic properties of the aryl substituents. BNNTs functionalized with aryl groups tethering electron-donating groups exhibited further redshifted CC PL, and the emission energies showed a preliminary substituent-dependent trend with the Hammett substituent constants for the functionalized aryl groups. These results suggest that the electronic nature of the functionalized aryl groups can influence the defect states responsible for the CC PL. The origin of this substituent dependence, however, is not captured by the present ground-state PBE calculations and remains to be clarified using excited-state theoretical approaches.

This study demonstrates that reductive arylation is an effective strategy for introducing an sp^3 boron defect to produce luminescent CCs in BNNTs and to tune their optical properties through control of the defect density and aryl substituent structure. This molecular defect-engineering approach provides a new platform for band structure modulation in BNNTs. The present BNNT CCs emit in the UV–visible region, which is attractive for UV–visible nanophotonic and anti-counterfeiting applications. In addition, the chemically produced defects demonstrated in this study provide a useful model system for understanding defect-state formation in wide bandgap BN nanomaterials. Although single-photon emission properties and single-nanotube spectroscopy were not evaluated in the present study, such investigations will be necessary to assess the potential of BNNT CCs for advanced optical and quantum photonic applications. Moreover, the emission wavelength of BNNT CCs may be extendable toward longer wavelength regions, including the infrared region, as suggested by a recent simulation study [11].

4 | Experimental Section

4.1 | Purification of BNNTs

The BNNT solid was placed in a ceramic crucible and heated at 800 °C in air for 2 h. After cooling to room temperature, the solid was washed with hot water and dried under vacuum, providing purified BNNTs [10].

4.2 | Synthesis of ph-BNNTs

To a 100 mL two-neck flask dried under vacuum with heat-gun heating, BNNTs (7.0 mg), sodium (65 mg), naphthalene (387 mg, 3.02 mmol), and dry THF (20 mL) were added in a nitrogen atmosphere. The mixture was sonicated for 1 h and stirred for 24 h at room temperature. After adding bromobenzene (0.21 mL, 2.01 mmol), the mixture was further stirred for 48 h at room temperature. The reaction was quenched by adding methanol and water, and precipitates were collected by filtration and washed with water, methanol, THF, and dichloromethane. The obtained solid was dried under vacuum for 15 h at 80 °C, which provided a colorless powder (ph-BNNTs). The other functionalized BNNTs were synthesized under similar reaction conditions using different bromobenzene derivatives.

23670932, 2026, 10, Downloaded from https://chemistry-europe.onlinelibrary.wiley.com/doi/10.1002/cptc.70316 by National Institute For, Wiley Online Library on [15/10/2026]. See the Terms and Conditions (https://onlinelibrary.wiley.com/terms-and-conditions) on Wiley Online Library for rules of use; OA articles are governed by the applicable Creative Commons License

4.3 | Solubilization of ph-BNNTs in an Aqueous CTAB Solution

The ph-BNNT solid (0.10 mg) and aqueous CTAB solution (0.010 wt%, 5.0 mL) were mixed in a 20 mL glass bottle and sonicated for 10 min, followed by centrifugation at 12,000 g for 1 h. A supernatant (top 80%) was collected as a ph-BNNT solution. BNNTs were also solubilized by the same procedure.

4.4 | DFT Calculations

DFT calculations were performed using VASP on the Genkai supercomputer. The GGA with the PBE exchange–correlation functional was employed. The present calculations were intended to compare relative changes in the ground-state electronic structure induced by functionalization rather than to reproduce absolute bandgap or PL transition energies. The plane-wave cutoff energy was set to 400 eV. A single-walled zigzag (10,0) BNNT consisting of 240 atoms, including 120 B atoms and 120 N atoms, was used as a computationally tractable model to isolate the local electronic structure changes induced by functionalization. This model was not intended to quantitatively reproduce the diameter or wall number distribution of the experimental BNNT samples. After structural optimization, the band structure of the pristine BNNT was calculated. For the phenyl-functionalized BNNT model, one phenyl group was introduced into one BNNT unit. An additional hydrogen atom was added to saturate the dangling bond generated by the phenyl addition. Possible hydrogen addition sites near the phenyl-functionalized site were examined, and the most stable optimized structure was used for the band structure calculation. The band structures and wave functions were visualized using VASPKIT. The calculated Kohn–Sham bandgaps were used only to discuss qualitative trends in the ground-state electronic structure among the model systems and were not directly assigned to PL transition energies.

Acknowledgments

This work was supported by Grants-in-Aid for JSPS KAKENHI grant numbers JP23K23178, JP24H01198, JP24K01279, and JP25K22300, JST CREST JPMJCR25A, JSPS grant number JPJSBP120249003, and JACI Prize for Outstanding Achievements. This work was supported by "Advanced Research Infrastructure for Materials and Nanotechnology in Japan (ARIM)" of the Ministry of Education, Culture, Sports, Science and Technology (MEXT). The computation was carried out using the computer resource offered under the category of General Projects by Research Institute for Information Technology, Kyushu University.

Funding

This study was supported by Japan Society for the Promotion of Science (Grant JSPS KAKENHI, JP23K23178, JP24H01198, JP24K01279, JP25K22300 and JPJSBP120249003), Japan Science and Technology Agency (Grant CREST JPMJCR25A), and Japan Association for Chemical Innovation (Grant JACI Prize for Outstanding Achievements).

Conflicts of Interest

The authors declare no conflicts of interest.

Data Availability Statement

The data that support the findings of this study are available from the corresponding author upon reasonable request.

References

1. A. Rubio, J. L. Corkill, and M. L. Cohen, "Theory of Graphitic Boron Nitride Nanotubes," *Physical Review B* 49 (1994): 5081–5084, https://doi.org/10.1103/PhysRevB.49.5081.

2. X. Blase, A. Rubio, S. G. Louie, and M. L. Cohen, "Stability and Band Gap Constancy of Boron Nitride Nanotubes," *Europhysics Letters* 28 (1994): 335–340, https://doi.org/10.1209/0295-5075/28/5/007.

3. N. G. Chopra, R. J. Luyken, K. Cherrey, et al., "Boron Nitride Nanotubes," *Science* 269 (1995): 966–967, https://doi.org/10.1126/science.269.5226.966.

4. K. Watanabe, T. Taniguchi, and H. Kanda, "Direct-Bandgap Properties and Evidence for Ultraviolet Lasing of Hexagonal Boron Nitride Single Crystal," *Nature Materials* 3 (2004): 404–409, https://doi.org/10.1038/nmat1134.

5. L. Museur and A. Kanaev, "Near Band-Gap Electronics Properties and Luminescence Mechanisms of Boron Nitride Nanotubes," *Journal of Applied Physics* 118 (2015): 084305, https://doi.org/10.1063/1.4928835.

6. A. Pierret, H. Nong, F. Fossard, et al., "Role of Structural Defects in the Ultraviolet Luminescence of Multiwall Boron Nitride Nanotubes," *Journal of Applied Physics* 118 (2015): 234307, https://doi.org/10.1063/1.4937990.

7. S. X. Li, T. Ichihara, H. Park, et al., "Prolonged Photostability in Hexagonal Boron Nitride Quantum Emitters," *Communications Materials* 4 (2023): 19, https://doi.org/10.1038/s43246-023-00345-8.

8. G. Cheng, S. Yao, X. Sang, et al., "Evolution of Irradiation-Induced Vacancy Defects in Boron Nitride Nanotubes," *Small* 12 (2016): 818–824, https://doi.org/10.1002/smll.v12.6.

9. M. Hennessey, B. Whitefield, P. Singh, et al., "Engineering Boron Vacancy Defects in Boron Nitride Nanotubes," *ACS Applied Materials & Interfaces* 16 (2024): 57552–57557, https://doi.org/10.1021/acsami.4c12802.

10. T. Shiraki, R. Saito, H. Saeki, N. Tanaka, K. Harano, and T. Fujigaya, "Defect Photoluminescence From Alkylated Boron Nitride Nanotubes," *Chemistry Letters* 52 (2023): 44–47, https://doi.org/10.1246/cl.220467.

11. S. Lee, J. Fortner, and Y. H. Wang, "Defect Pairs in Boron Nitrides That Exhibit Strong Electronic Transitions in the Infrared," *Journal of Physical Chemistry C* 128 (2024): 11672–11678, https://doi.org/10.1021/acs.jpcc.4c01586.

12. J. Chattopadhyay, A. K. Sadana, F. Liang, et al., "Carbon Nanotube Salts. Arylation of Single-Wall Carbon Nanotubes," *Organic Letters* 7 (2005): 4067–4069, https://doi.org/10.1021/ol050862a.

13. Y. Maeda, Y. Iguchi, P. Zhao, et al., "Switching Photoluminescence Wavelength of Arylated Single-Walled Carbon Nanotubes by Utilizing Steric Hindrance in Reductive Arylation," *Chemistry – A European Journal* 31 (2025): e202404529, https://doi.org/10.1002/chem.v31.13.

14. C. A. de los Reyes, K. L. W. Mitra, A. D. Smith, et al., "Chemical Decoration of Boron Nitride Nanotubes Using the Billups-Birch Reaction: Toward Enhanced Thermostable Reinforced Polymer and Ceramic Nanocomposites," *ACS Applied Nano Materials* 1 (2018): 2421–2429, https://doi.org/10.1021/acsanm.8b00633.

15. B. J. Mapleback, N. Brack, L. Thomson, et al., "Development of Stable Boron Nitride Nanotube and Hexagonal Boron Nitride Dispersions for Electrophoretic Deposition," *Langmuir* 36 (2020): 3425–3438, https://doi.org/10.1021/acs.langmuir.0c00018.

16. H. Shin, J. Guan, M. Z. Zgierski, K. S. Kim, C. T. Kingston, and B. Simard, "Covalent Functionalization of Boron Nitride Nanotubes via

23670932, 2026, 10, Downloaded from https://chemistry-europe.onlinelibrary.wiley.com/doi/10.1002/cptc.70316 by National Institute For, Wiley Online Library on [15/10/2026]. See the Terms and Conditions (https://onlinelibrary.wiley.com/terms-and-conditions) on Wiley Online Library for rules of use; OA articles are governed by the applicable Creative Commons License

Reduction Chemistry," *ACS Nano* 9 (2015): 12573–12582, https://doi.org/10.1021/acsnano.5b06523.

17. Y. Piao, B. Meany, L. R. Powell, et al., "Brightening of Carbon Nanotube Photoluminescence Through the Incorporation of sp^3 Defects," *Nature Chemistry* 5 (2013): 840–845, https://doi.org/10.1038/nchem.1711.

18. B. J. Gifford, X. He, M. Kim, et al., "Optical Effects of Divalent Functionalization of Carbon Nanotubes," *Chemistry of Materials* 31 (2019): 6950–6961, https://doi.org/10.1021/acs.chemmater.9b01438.

Supporting Information

Additional supporting information can be found online in the Supporting Information section.

23670932, 2026, 10, Downloaded from https://chemistry-europe.onlinelibrary.wiley.com/doi/10.1002/cptc.70316 by National Institute For, Wiley Online Library on [15/10/2026]. See the Terms and Conditions (https://onlinelibrary.wiley.com/terms-and-conditions) on Wiley Online Library for rules of use; OA articles are governed by the applicable Creative Commons License